A Putative Consensus Sequence for the Nucleotide-Binding Site of Annexin A6[†]

Joanna Bandorowicz-Pikula,*[,‡] Aneta Kirilenko,[‡] Ruud van Deursen,[§] Marcin Golczak,[‡] Michael Kühnel,[||] Jean-Marc Lancelin,[||] Slawomir Pikula,[‡] and René Buchet[§]

Department of Cellular Biochemistry, Nencki Institute of Experimental Biology, 02-093 Warsaw, Poland, Laboratoire de RMN Biomoléculaire associé au CNRS, Université Claude Bernard, Lyon 1, UFR de Chimie-Biochimie, Ecole Supérieure de Chimie Physique Electronique de Lyon, F-69622 Villeurbanne, France, and Laboratoire de Physico-Chimie Biologique, UMR CNRS 5013, Université Claude Bernard, Lyon 1, UFR de Chimie-Biochimie, F-69622 Villeurbanne, France

Received March 6, 2003; Revised Manuscript Received May 27, 2003

ABSTRACT: Reaction-induced infrared difference spectroscopy (RIDS) has been used to investigate the nature of interactions of human annexin A6 (ANXA6) with nucleotides. RIDS results for ANXA6, obtained after the photorelease of GTP-γ-S, ATP, or P_i from the respective caged compounds, were identical, suggesting that the interactions between the nucleotide and ANXA6 were dominated by the phosphate groups. Phosphate-induced structural changes in ANXA6 were small and affected only seven or eight amino acid residues. The GTP fluorescent analogue, 2′(3′)-*O*-(2,4,6-trinitrophenyl)guanosine 5′-triphosphate (TNP-GTP), quenched tryptophan fluorescence of ANXA6 when bound to the protein. A binding stoichiometry of 1 mol of nucleotide/mol ANXA6 was established with a K_D value of 2.8 μM for TNP-GTP. The bands observed on RIDS of ANXA6 halves (e.g., N-terminal half, ANXA6a, and C-terminal half, ANXA6b) were similar to those of the whole molecule. However, their amplitudes were smaller by a factor of 2 compared to those of whole ANXA6. TNP-GTP bound to both fragments of ANXA6 with a stoichiometry of 0.5 mol/mol. However, the binding affinities of ANXA6a and ANXA6b differed from that of ANXA6. Simulated molecular modeling revealed a nucleotide-binding site which was distributed in two distinct domains. Residues K296, Y297, K598, and K644 of ANXA6 were less than 3 Å from the bound phosphate groups of either GTP or ATP. The presence of two identical sequences in ANXA6 with the F-X-X-K-Y-D/E-K-S-L motif, located in the middle of ANXA6, at residues 293−301 (within ANXA6a) and at 641−649 (within ANXA6b), suggested that the F-X-X-K-Y-D/E-K-S-L motif was the putative sequence in ANXA6 for nucleotide binding.

Annexins belong to a family of homologous Ca^{2+}- and phospholipid-binding proteins. They are represented in various verterbrate tissues by at least 12 different subfamilies (*1*). Among these, the eight-repeat domain annexin, ANXA6, is the largest (M_r = 68 kDa) member of the family (*1*). Analysis of paralogy linkage maps between human chromosomes 4 and 5, and the comparison of primary sequences of several annexins, suggest that the four-repeat domain annexins, ANXA5 and ANXA10, may be the direct progenitors of ANXA6 octad formation (*1*). Experimental evidence indicates that mammalian ANXA6 may bind ATP and GTP *in vitro* (*2*−*5*) and that a putative nucleotide-binding domain is located in the N-terminal half of the annexin molecule (*5*, *6*). However, the functional significance of these findings, and the primary structure of the nucleotide-binding domain in ANXA6, remained uncertain (*7*).

On the basis of its known properties and its intracellular localization, it has been proposed that ANXA6 may be involved in nucleotide-dependent processes, such as membrane trafficking (*8*), signal transduction pathways within specific membrane microdomains (*9*), and canalicular contraction in hepatocyte (*10*). It has been observed that ANXA6 interacts or colocalizes with GTP-binding proteins, e.g., a GTPase [dynamin (*11*)], and proteins mediating vesicle docking and/or fusion (e.g., v-SNARE, VAMP-2, and NSF) (*12*) or with GTPase activating proteins (GAPs, e.g., $p120^{GAP}$) (*13*, *14*). Plant annexins from maize, tomato, and cotton can hydrolyze nucleotides (*15*−*17*). This hydrolytic activity has been suggested to play a role in vesicular transport in plant cells (*15*−*18*). The hydrolytic activity toward ATP (determined by the analysis of the monophosphate generated from ATP) has been reported for annexin 24 (Ca32) from *Capsicum annum*; this activity is slightly activated by Ca^{2+} but completely vanishes in the presence of a divalent cation chelating agent (*19*). In the case of mammalian annexins, the best example of proteins displaying both GTP binding properties and GTPase activity is ANXA7 from chromaffin (*20*−*23*) and alveolar type II cells (*24*). In chromaffin cells, GTP-activated ANXA7 has been implicated

[†] This work was supported by grants from the Polish State Committee for Scientific Research (Grant 3 P04A 007 22 to J.B.-P.), from the French Ministry of Research (senior research fellowship to J.B.-P.), and from CNRS.

* To whom correspondence should be addressed: Department of Cellular Biochemistry, Nencki Institute of Experimental Biology, 3 Pasteur St., 02-093 Warsaw, Poland. Phone: 48-22-659-8571, ext. 347. Fax: 48-22-822-53-42. E-mail: bandor@nencki.gov.pl.

[‡] Nencki Institute of Experimental Biology.

[§] Laboratoire de Physico-Chimie Biologique, UMR CNRS 5013, Université Claude Bernard.

[||] Laboratoire de RMN Biomoléculaire associé au CNRS, Université Claude Bernard.

10.1021/bi034359m CCC: $25.00
Published on Web 07/09/2003

in exocytotic membrane fusion (*21*, *23*) and surfactant secretion (*24*). For other mammalian annexins, such as ANXA5 (*19*) and ANXA6 (*25*), the hydrolytic activity toward nucleotides has been questioned.

In this report, we have used RIDS[1] (*26*−*30*) to investigate the molecular details of the peptide backbone structure, the side chain environment, and the nature of the nucletide-binding site. Furthermore, RIDS in combination with fluorescence spectroscopy and simulated molecular modeling permitted us to localize the nucleotide-binding domain of ANXA6. The nucleotide binding, characterized by RIDS and fluorescence spectroscopy, was observed in the whole protein, and in the N-terminal (ANXA6a) and C-terminal (ANXA6b) halves of ANXA6. This result suggested that the nucleotide-binding site of ANXA6 is formed by the amino acid residues located in both halves of the protein. Simulated molecular modeling was performed in a limited region of ANXA6, consistent with experimental results. K296, Y297, K598, and K644 were found to be less than 3 Å from β- and γ-phosphate groups of either GTP or ATP. Two identical sequences with the F-X-X-K-Y-D/E-K-S-L motif, residues 293−301 (within ANXA6a) and 641−649 (within ANXA6b), were identified.

MATERIALS AND METHODS

Materials. The caged compounds, ATP[Et($PhNO_2$)], PO_4[Et($PhNO_2$)], GTP-γ-S[1-(4,5-dimethoxy-2-nitrophenyl)-ethyl], and the fluorescent GTP analogue, 2′(3′)-*O*-(2,4,6-trinitrophenyl)guanosine 5′-triphosphate (TNP-GTP), were obtained from Molecular Probes Inc. (Eugene, OR). GTP, GTP-agarose (3.0 μmol of GTP/mL of packed resin), and V8 protease from *Staphylococcus aureus* were purchased from Sigma-Aldrich (Poznan, Poland). Isopropyl β-D-thiogalactopyranoside (IPTG) was provided by BIO 101, Inc. (Vista, CA), and acrylamide by Bio-Rad (Richmond, CA). All other chemicals of the highest purity were commercially available.

Preparation of Recombinant Proteins. Human recombinant annexin ANXA6, and its peptide fragments ANXA6a (residues 2−342) and ANXA6b (residues 348−673), were expressed in *Escherichia coli* strain B121(DE3) after induction with IPTG and purified to homogeneity, using the protocol described for the purification of ANXA5 (*31*), with small modifications (*32*, *33*). Detachment of ANXA6 and its fragments from liposomes (prepared from bovine brain lipid extract) was achieved by incubation of proteins and liposomes in 20 mM Tris-HCl buffer (pH 8.0), 100 mM NaCl, 10 mM EGTA, and 3 mM $MgCl_2$, followed by separation of the liposomes from the proteins by centrifugation at 100000*g* for 40 min at 4 °C. The supernatants containing proteins were collected, dialyzed against 20 mM Tris-HCl buffer (pH 8.3) and 0.1 mM EGTA, and loaded onto a Q-Sepharose column for further purification. ANXA6 or its fragments were eluted from the column with a linear gradient of NaCl (from 0 to 500 mM NaCl). ANXA6 and ANXA6a eluted with the fractions containing 300−400 mM NaCl, while ANXA6b eluted with the fractions containing 200−250 mM NaCl. Final purifications of ANXA6 and ANXA6a were achieved by hydroxyapatite column chromatography. Fractions containing the respective peptides were dialyzed against 10 mM phosphate buffer (pH 7.4) and 0.1 mM EGTA, loaded on a column by gravity, and eluted at pH 7.4 by using a linear gradient of phosphate buffer concentrations. ANXA6 and ANXA6a were recovered in fractions eluted with 230−250 mM phosphate buffer. Corresponding cDNAs encoding ANXA6a and ANXA6b subcloned into the pRSET-5d plasmid were sequenced by the dideoxy chain termination procedure, using a double-stranded plasmid DNA (*34*). The sequencing primer ACAACGGTTTCCCTCTAG, complementary to the pRSET-5d sequence, was generated using Gene Runner software (version 3.0, Hasting Software Inc.) and then synthesized. The digestion of ANXA6 with V8 protease in the presence of GTP-agarose was performed, as described previously (*5*, *6*). The proteolytic fragments of ANXA6 were subjected to SDS−PAGE and electroblotted onto a PVDF membrane for direct sequencing. The peptide sequencing was performed by the Protein Chemistry Laboratory of Jagiellonian University (Cracow, Poland).

Preparation of Samples for RIDS. ANXA6, ANXA6a, or ANXA6b was lyophilized and dissolved in ^2H_2O buffer containing 100 mM Tris-HCl buffer (pD 7.5), 2 mM $CaCl_2$, or 1 mM EGTA and 2 mM caged compound {either ATP[Et($PhNO_2$)], PO_4[Et($PhNO_2$)], or GTP-γ-S[1-(4,5-dimethoxy-2-nitrophenyl)ethyl]}, corresponding to a maximum of 1.6 mM photoreleased ligand after UV illumination. A sample containing 10 mM GTP, to saturate the nucleotide-binding site of ANXA6, was used as an additional control. The protein concentration of ANXA6, ANXA6a, and ANXA6b was 100 μM. The pD was determined with a glass electrode and was corrected by a value of 0.4 (*35*). The same buffer without protein was used to measure the infrared absorption of caged compound and its photoproduct. All samples were freshly prepared and incubated for 5 min in the dark at room temperature before Fourier transform infrared (FTIR) spectra measurement.

FTIR Difference Spectroscopic Measurements. Infrared data were acquired with a Nicolet 510M FTIR spectrometer equipped with a DTGS detector, using a temperature-controlled flow-through cell (model TFC-M25, Harrick Scientific Corp., Ossining, NY) with 50 μm spacers and CaF_2 windows. The infrared spectra were recorded at 20 °C with 256 interferograms each at 4 cm^{-1} resolution and Fourier transformed. During data acquisition, the spectrometer was continuously purged with dry filtered air (Balston regenerating desiccant dryer, model 75-45 12 VDC). Once the infrared spectrum was recorded, the sample was exposed to UV illumination (150 W Xe−Hg lamp) for 120 s that induced the photorelease of the nucleotide or P_i from the respective caged compound, allowing it to bind to ANXA6, ANXA6a, or ANXA6b. Five minutes after illumination, a second FTIR spectrum was recorded under the same conditions. The RIDS spectrum of the sample was obtained by subtracting the first FTIR spectrum (before illumination) from the second FTIR spectrum (after illumination). Positive bands indicated the formation of new structures or molecular interactions due

[1] Abbreviations: ANXA, mammalian annexin; ANXA6a, N-terminal half of annexin A6; ANXA6b, C-terminal half of annexin A6; caged-ATP, ATP[Et($PhNO_2$)]; CD, circular dichroism; FRET, fluorescence resonance energy transfer; FTIR, Fourier transform infrared spectroscopy; caged-GTP-γ-S, GTP-γ-S[1-(4,5-dimethoxy-2-nitrophenyl)ethyl]; GTP-γ-S, guanosine 5′-3-*O*-(thio)triphosphate; IPTG, isopropyl β-D-thiogalactopyranoside; caged-P_i, PO_4[Et($PhNO_2$)]; RIDS, reaction-induced infrared difference spectroscopy; TNP-GTP, 2′(3′)-*O*-(2,4,6-trinitrophenyl)guanosine 5′-triphosphate.

to the binding of the photoreleased ligand, while negative bands reflected the disappearance of structures or molecular interactions that were present in the protein before binding of the ligand. For each experiment, three to nine individual RIDS spectra were measured under the same conditions. They were added and averaged to obtain the final RIDS spectrum with a better signal-to-noise ratio. The final RIDS spectrum was corrected for water vapor absorption but was not smoothed. The number of amino acid residues involved in the nucleotide-binding site of ANXA6 and its halves was computed from the relative intensity ratio of the infrared band in the amide I region (*36*). Although the numbers that were obtained serve as an estimate of the magnitude of infrared changes, the method of their calculation constitutes a straightforward approach to comparing quantitative changes between different samples. The number of residues involved is a lower estimate because of band overlapping, resulting in smaller infrared difference spectra (*36*, *37*).

Steady-State Fluorescence Measurements. The fluorescence of ANXA6 was monitored at 25 °C using a Fluorolog 3 spectrophotometer (Jobin Yvon Spex, Edison, NJ) at 3 nm resolution for excitation and emission. The 5 × 5 mm cuvettes with an internal volume of 0.6 mL contained 50 mM Tris-HCl buffer (pH 7.4), 0−3.5 μM ANXA6, 0−15 μM TNP-GTP, 50 mM NaCl, and 2 mM $CaCl_2$ or 1 mM EGTA. TNP-GTP fluorescence emission (500−600 nm) spectra were recorded after excitation of samples at 415 nm. Fluorescence titrations with various nucleotide concentrations were monitored at λ_{em}s of 545 and 550 nm (λ_{ex} was 415 nm). Dilution did not exceed 10%, and the fluorescence intensity was corrected for the dilution factor. Background emission of buffer containing the ligand and no protein was subtracted from the protein signal. To minimize inner filter effects, the total absorbance of the protein/ligand mixtures was not allowed to exceed 0.2 absorbance unit. To compensate for the decrease in fluorescence due to the increased absorption of TNP-GTP, the measured fluorescence was corrected by a factor $f(\Delta A_1,\Delta A_2)$ equal to $10^{(\Delta A_1+\Delta A_2)/2}$. ΔA_1 and ΔA_2 are the increases in absorption at the excitation and emission wavelengths, respectively, upon addition of the ligand (*38*). The specific fluorescence change (ΔF) of TNP-GTP, corresponding to the binding of the nucleotide to ANXA6, was obtained by subtracting the nonspecific fluorescence measured in the presence of 5 mM GTP from the total fluorescence. To obtain dissociation constants (K_Ds), the ΔF values were plotted versus TNP-GTP concentrations (D_0). The experimental points were fitted using eq 1 (*39*)

$$\Delta F = \Delta F_{max}\{U_0 + D_0 + K_D - [(U_0 + D_0 + K_D)^2 - 4U_0D_0]^{1/2}\}/(2U_0) \quad (1)$$

where U_0 is the concentration of ANXA6 (in micromolar) and ΔF_{max} is the maximal specific fluorescence increase. The stoichiometry (n) of binding of TNP-GTP to ANXA6 was determined from the mass action plot, based on the following rationale (*40*):

$$r/[L]_{free} = n/K_D - r/K_D \quad (2)$$

where r is the ratio of the bound ligand concentration to the ANXA6 concentration and $[L]_{free}$ the concentration of the free ligand. Fluorescence resonance energy transfer (FRET) between protein tryptophan residues and the nucleotide was assessed after excitation of ANXA6 in the presence or absence of TNP-GTP. The samples were excited at 295 nm, and the emission spectra were recorded at wavelengths from 305 to 580 nm. The emission and excitation slits were set at 2 and 3 nm, respectively.

Molecular Simulations. Bovine ANXA6 coordinates (*41*) were retrieved from the Protein Data Bank (PDB entry 1AVC). The numbering of amino acid residues was based on the full sequence containing the initial M. To find possible binding sites, PASS (Putative Active Sites with Spheres) software was used to calculate the volumes of the possible sites for an indication of ligand access (*42*). On the basis of these results, a box with an edge length of 2.2 nm was defined around the most accessible site of ANXA6. Within this box, the nucleotide was allowed to move freely, whereas ANXA6 was fixed on a grid during further calculations.

The software AUTODOCK computed the free energy of the interaction between nucleotide and ANXA6, based on a genetic algorithm (*43*). A set of solutions, corresponding to the minimal free energy values, were selected, together with the corresponding coordinates of the nucleotide within the active site of ANXA6. Visualization software, RASMOL and SYBYL (Tripos Inc.), was used to identify the active site, the coordination of the ligand, and the involved residues.

Miscellaneous Methods. Protein concentrations were determined by the method of Bradford (*44*) with bovine serum albumin as a standard. Ca^{2+} concentrations were calculated using the Chelator program (*45*). SDS−PAGE (under reducing conditions) was performed on 5% stacking and 7.5 or 12% resolving gels; gels were stained with Coomassie brilliant blue (*46*).

RESULTS

Evidence of Interaction between ANXA6 and Phosphate Groups of the Nucleotide. Previous infrared and fluorecence results have shown that ATP and GTP can bind to mammalian ANXA6 (*2*−*5*). During the study presented here, infrared spectroscopy in combination with caged-GTP-γ-S was employed to further delineate the mechanisms of nucleotide binding to ANXA6. After illumination and photolysis, GTP-γ-S (nonhydrolyzable analogue of GTP) was released from its bulky cage, resulting in the interaction with ANXA6. Consequently, by measurement of infrared difference spectra before and after illumination, it was possible to monitor small structural changes caused by the interactions between the GTP-γ-S group and amino acid residues of ANXA6. Negative bands correspond to vibrational modes of chemical groups which disappeared after photolysis, while the positive bands indicated the appearance of new vibrational groups. The photorelease of GTP-γ-S from its cage produced RIDS spectra (Figure 1, trace a) indicating a new band located at ~1687 cm^{-1} and a concomitant decrease in the magnitude of the band at 1529 cm^{-1}. This corresponded to the formation of a carbonyl group in the photoproduct and the disappearance of a nitro group (*27*). The RIDS spectrum of 100 μM ANXA6 and caged-GTP-γ-S (Figure 1, trace b) exhibited four additional bands located at 1656, 1621, 1579, and 1545 cm^{-1}, as compared to the photolysis spectrum of caged-GTP-γ-S. The difference spectrum between two RIDS spectra (trace b minus trace a in Figure 1)

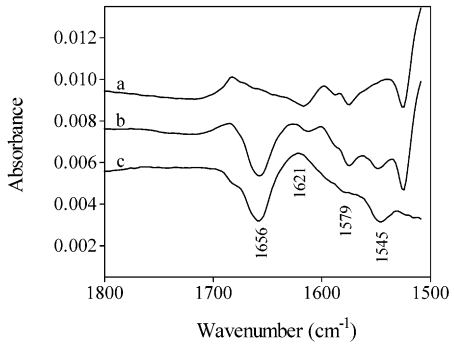

FIGURE 1: Structural changes induced by binding of GTP-γ-S to ANXA6. Difference infrared spectra obtained after photorelease of GTP-γ-S from its precursor, caged-GTP-γ-S, in the absence of ANXA6 (trace a) and in the presence of 100 μM ANXA6 (trace b). The ^2H_2O buffer was composed of 2 mM caged-GTP-γ-S, 100 mM Tris-HCl (pD 7.5), and 2 mM $CaCl_2$. Trace c represents a difference spectrum (trace b minus trace a), reflecting uniquely GTP-γ-S-induced structural changes of ANXA6. Each trace represents the average of eight or nine individual RIDS spectra.

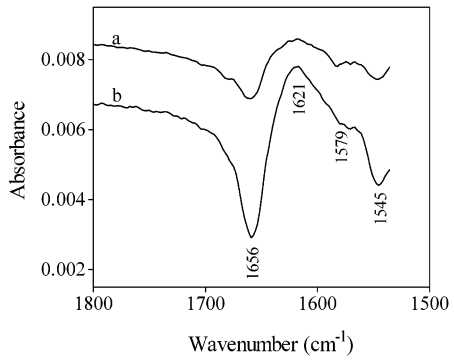

FIGURE 2: Inhibition of binding of GTP-γ-S to ANXA6 by a saturated amount of GTP. Difference infrared spectra after photorelease of GTP-γ-S from its precursor, caged-GTP-γ-S, in the presence of 100 μM ANXA6 with (trace a) or without (trace b) 10 mM GTP. The ^2H_2O buffer was composed of 100 mM Tris-HCl (pD 7.5), 2 mM caged-GTP-γ-S, and 2 mM $CaCl_2$. Each trace represents the average of eight or nine individual RIDS spectra. The bands associated with the photolysis-released nucleotide were subtracted from their respective RIDS spectra as indicated in Figure 1. Only the bands induced by the binding of GTP-γ-S to ANXA6 are shown.

corresponded solely to GTP-γ-S binding to ANXA6 (Figure 1, trace c; see also ref *5*). In controls, 10 mM GTP was added to prevent binding of GTP-γ-S to ANXA6. A significant decrease in the magnitudes of infrared signals was observed in the case of ANXA6 containing GTP (Figure 2, trace a), as compared with the sample without GTP (Figure 2, trace b). Therefore, the 1656, 1621, 1579, and 1545 cm^{-1} bands (Figure 2, trace b) were assigned to structural changes in ANXA6 induced by the binding of GTP-γ-S.

To identify the nature of the structural changes, other ligands such as ATP and phosphate were employed. The RIDS spectrum of a sample containing caged-P_i and ANXA6 (Figure 3, trace a) showed the presence of a positive band located at 1621 cm^{-1} and the three negative bands located at 1656, 1579, and 1545 cm^{-1}. These bands are caused by the photorelease of P_i in the presence of ANXA6. The 1621 and 1656 cm^{-1} bands are characteristic for carbonyl groups of the peptide backbone (*47*−*52*), reflecting slight structural changes, caused by the phosphate binding to the protein. The 1579 cm^{-1} band corresponds to the carboxylate group of side

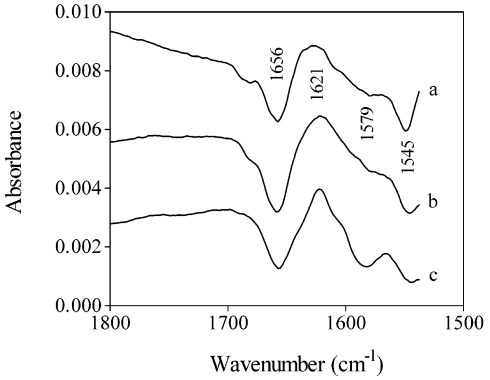

FIGURE 3: Comparison of nucleotide (ATP and GTP-γ-S) and P_i binding sites in ANXA6 as probed by reaction-induced infrared spectroscopy. RIDS of 100 μM ANXA6 in ^2H_2O buffer containing 100 mM Tris-HCl (pD 7.5) and 2 mM $CaCl_2$ with either 2 mM caged-P_i (trace a), 2 mM caged-GTP-γ-S (trace b), or 2 mM caged-ATP (trace c). Each trace represents the average of eight or nine individual RIDS spectra. The bands associated with the photolysis-released nucleotide or P_i were subtracted from their respective RIDS spectra. Only changes in the bands induced by the binding of nucleotide or P_i to ANXA6 are presented.

Table 1: Estimated Number of Amino Acid Residues in the Nucleotide-Binding Site of ANXA6 and Its Fragments ANXA6a and ANXA6b, Calculated via RIDS

protein	ligand	additions	no. of residues
ANXA6	caged-GTP	2 mM $CaCl_2$	8−9
ANXA6	caged-GTP	1 mM EGTA	5−6
ANXA6	caged-GTP	2 mM $CaCl_2$ and 10 mM GTP	3−4
ANXA6a	caged-GTP	2 mM $CaCl_2$	4−5
ANXA6b	caged-GTP	2 mM $CaCl_2$	3−4
ANXA6	caged-ATP	2 mM $CaCl_2$	7−8
ANXA6	caged-P_i	2 mM $CaCl_2$	6−7

chain residues of either the D or E residue (*53*−*55*), suggesting that the interactions between phosphate and ANXA6 involved either D or E residues. Alternatively, it may be related to the NH group being either exposed to the deuterated solvent or affected by the nucleotide binding. The negative band at 1545 cm^{-1} may suggest a slight exposure of NH groups to the deuterated solvent, although a contribution from the carboxylate group cannot be ruled out. The buried NH groups of the peptide backbone, not accessible to solvent, became exposed after phosphate binding. The exposed NH groups exchanged their protons with a deuterium from the solvent, indicating that the binding of phosphate promotes small movements of protein domains.

The RIDS spectrum of caged-P_i in the presence of ANXA6 reflected interactions of the phosphate chain with the protein (Figure 3, trace a) that were similar to those observed in the case of photolysis of caged-GTP-γ-S (Figure 3, trace b; see also ref *5*). These results suggested that the RIDS spectrum of a sample containing ANXA6 and caged-GTP-γ-S corresponded essentially to the interactions of the phosphate moiety of GTP-γ-S with the annexin. The calculated number of amino acid residues involved in phosphate binding to ANXA6 was 6 or 7, instead of 8 or 9 in the case of GTP-γ-S binding (Table 1). A fraction of caged-P_i was probably already bound to the protein prior to photolysis, despite the presence of its bulky residue. Comparison of the RIDS spectrum of ANXA6 with that of either caged-GTP-γ-S (Figure 3, trace b) or caged-ATP (Figure 3, trace c; see also

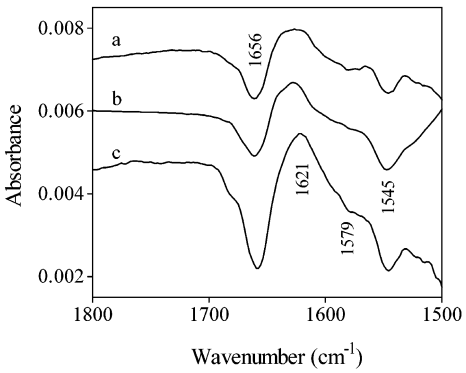

FIGURE 4: Comparison of difference infrared spectra induced by the photorelease of GTP-γ-S from caged-GTP-γ-S in samples containing either ANXA6 or its fragments. RIDS spectra of 100 μM ANXA6b (trace a), 100 μM ANXA6a (trace b), or 100 μM ANXA6 (trace c) with 2 mM caged-GTP-γ-S are shown. The ^2H_2O buffer was composed of 100 mM Tris-HCl (pD 7.5) and 2 mM $CaCl_2$. Each trace represents the average of three to nine individual RIDS spectra. The bands associated with the photolysis-released nucleotide (*4*, *5*) were deducted from their respective RIDS spectra. Only the bands induced by the binding of GTP-γ-S to ANXA6 or its fragments are shown.

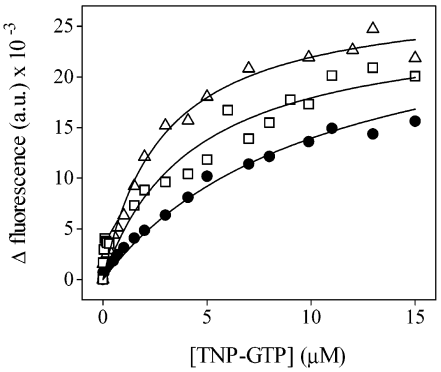

FIGURE 5: Binding of TNP-GTP to ANXA6. Fluorescence titrations of 2 μM ANXA6 (△), ANXA6a (□), or ANXA6b (●) with the indicated concentrations of TNP-GTP on the abscissa were performed. The buffer was composed of 50 mM Tris-HCl (pH 7.4), 50 mM NaCl, and 2 mM $CaCl_2$. Samples were excited at 415 nm, and fluorescence emission was monitored at 545 nm. All titrations were repeated twice. The results varied by 5−7%.

Table 2: Characteristics of Binding of TNP-GTP to ANXA6, ANXA6a, and ANXA6b in the Presence of 2 mM Ca^{2+}

peptide	λ_{em-max} (nm)[a]	increase in fluorescence intensity[b]	K_D (μm)[c]	n[d] (mol/mol)
ANXA6	548 ± 1	1.6-fold	2.8 ± 0.2	1.1 ± 0.1
ANXA6a	548 ± 2	1.5-fold	2.7 ± 0.2	0.5 ± 0.05
ANXA6b	550 ± 2	1.2-fold	16.3 ± 2.6	0.6 ± 0.05

[a] The λ_{em-max} of TNP-GTP in the absence of protein amounted to 553 ± 1 nm. [b] Related to the extrinsic fluorescence of free TNP-GTP. [c] Fluorescence measurements were performed at a λ_{em-max} and a λ_{ex} of 415 nm. [d] The stoichiometry of binding of TNP-GTP to ANXA6 or its fragments was calculated using the mass action plot described in detail in Materials and Methods.

ref *4*) revealed similar spectral features, confirming that the RIDS spectrum predominantly reflected the interaction of phosphate groups of the nucleotide with ANXA6. From these results, it was not possible to determine to how many phosphate groups of the nucleotide did bind to ANXA6. To overcome this shortcoming, we performed simulated molecular modeling (described below) which suggested that the γ- and β-phosphate groups of the nucleotide may be involved in the interaction with ANXA6.

Location of the Nucleotide-Binding Site of ANXA6. To probe the location of the nucleotide-binding site of ANXA6, the fragments of human recombinant ANXA6 were prepared. The structural changes caused by the binding of GTP-γ-S to ANXA6b (Figure 4, trace a) or ANXA6a (Figure 4, trace b) were found to be similar, as indicated by the RIDS spectra of these fragments in the presence of GTP-γ-S. The magnitude of their RIDS spectra was approximately half the magnitude of the RIDS spectrum of ANXA6 (Figure 4, trace c). It was estimated that three or four amino acid residues were involved in the binding of GTP-γ-S to ANXA6b. Approximately four or five amino acid residues were estimated to be involved in the binding of GTP-γ-S to ANXA6a (Table 1). These numbers were approximately half the number of amino acid residues involved in the binding of GTP-γ-S to ANXA6. Chelating of Ca^{2+} by EGTA reduced the number of amino acid residues involved in the nucleotide-binding site of ANXA6 (Table 1). This result suggests that calcium promoted the interaction of phosphate with ANXA6.

The location of the nucleotide-binding site of ANXA6 was also determined by measuring TNP-GTP fluorescence. The advantage of this experimental approach over RIDS and caged ligands is that it allows determination of binding constants for the ligands. The fluorescent nucleotide was found to bind recombinant ANXA6, ANXA6a, and ANXA6b in a hyperbolic manner as indicated by an enhancement of the extrinsic fluorescence of TNP-GTP (Figure 5) and a slight blue shift of its emission maximum in the presence of these proteins (Table 2). GTP released TNP-GTP very efficiently from ANXA6, and the concentration of GTP required for half-maximal release was found to be 4.2 mM. These results indicate that the TNP-GTP and TNP-ATP binding characteristics of human recombinant ANXA6 were similar to those of porcine liver ANXA6 (*4*). The stoichiometry of binding of TNP-GTP to ANXA6 was determined to be 1 mol of nucleotide/mol of protein, with a K_D value of 2.8 μM in the presence of Ca^{2+} (Table 2). The binding stoichiometry for ANXA6a and ANXA6b was found to be 0.5 mol/mol, which was consistent with the number of amino acid residues involved in GTP binding to ANXA6 halves, as determined by RIDS.

ANXA6a, containing the N-terminal part of the protein, including four repeat domains I/IV, exhibited K_D values for TNP-GTP similar to those of ANXA6. On the other hand, ANXA6b, comprising four repeat domains V/VIII, was found to bind TNP-GTP with an almost 10-fold lower efficiency than recombinant ANXA6 (Table 2). These results indicated that the lack of the N-terminal half of ANXA6, and most of the linker region between the two symmetrical lobes of ANXA6 where W343 is located, significantly prevented the binding of TNP-GTP to the protein. Consistent with this, by purification of V8 protease proteolytic fragments of ANXA6 by affinity chromatography on GTP-agarose, the major fragment for which M_r = 35 kDa, originating from N-terminal half of ANXA6, starting with A^2KPAQGAKYR..., was identified.

Docking Nucleotides on ANXA6 Reveals Two Nucleotide-Binding Domains with Similar Sequences. PASS software first allowed us to locate accessible cavities in bovine

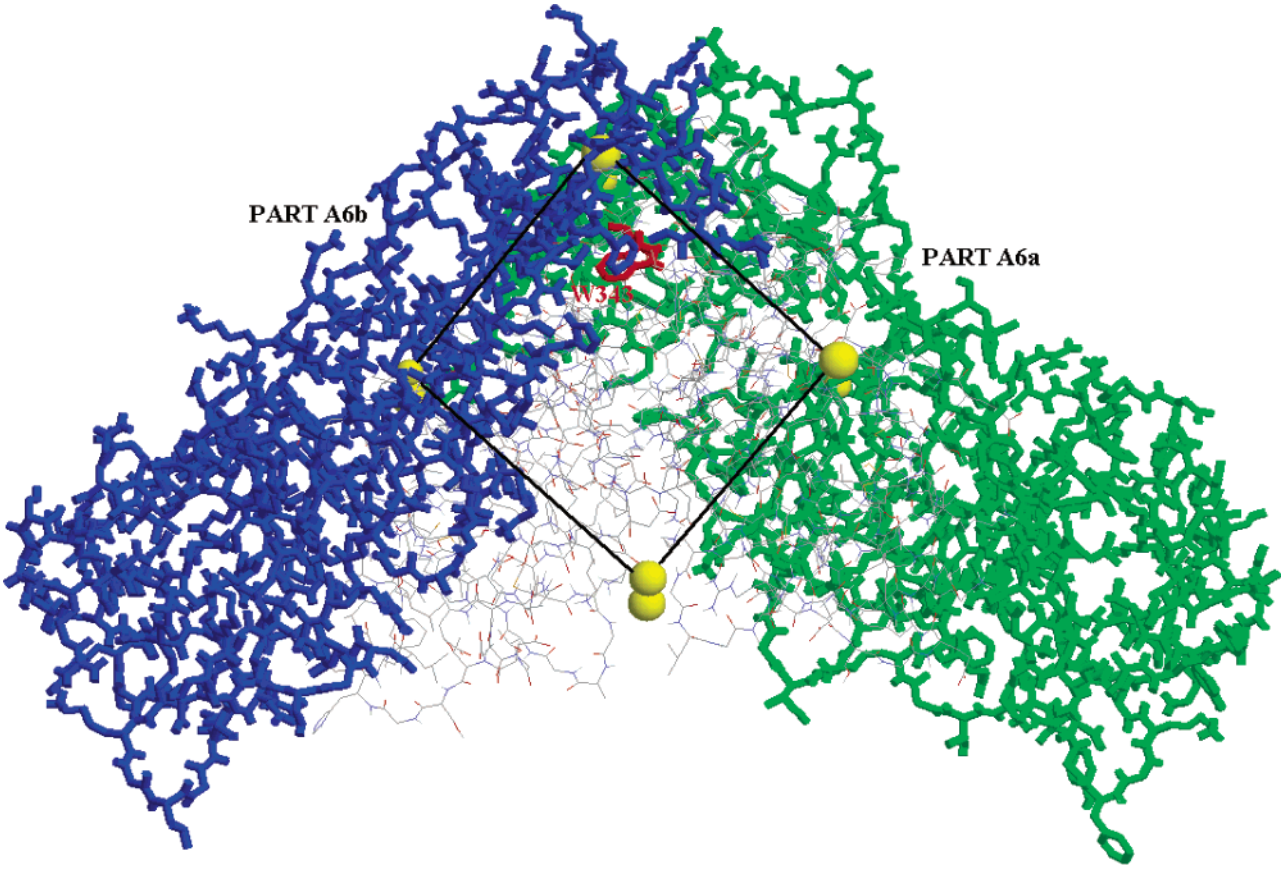

FIGURE 6: Bovine ANXA6 structure. Atomic coordinates were obtained from the Protein Data Bank (entry 1AVC). The N-terminal part of ANXA6 corresponding to residues 2−342 (ANXA6a) is shown in green, while the C-terminal part associated with residues 348−673 (ANXA6b) is shown in blue. The box with a limited dimension at the center of ANXA6 indicates the putative location of the nucleotide-binding site. Its approximate position is based on the accessibility of the cavity, as determined by PASS software (*42*), and on the intersection between the two halves: ANXA6a and ANXA6b. During the molecular simulation, the nucleotide was allowed to move freely inside the box.

ANXA6, where any type of ligand can bind. During the period of the preparation of this article, a crystal structure for human ANXA6 was deposited in the Protein Data Bank [PDB entry 1M9I, a phosphorylation-mimicking mutant T356D of ANXA6 (*56*)]. Despite a moderate crystallographic resolution of ca. 0.265 nm, the crystal structure of human ANXA6 superimposes on the bovine ANXA6 crystal structure with a root-mean-square deviation of less than 0.05 nm for the main chain N, Cα, and C′ atoms, indicating they are closely related structures. In addition, the orientations of any amino acid side chain within the possible interacting region (which has a good crystallographic order in both forms) have strictly the same orientational conformation. Since almost no differences were found either in amino acid sequences or in local conformations, the models obtained with the use of the bovine ANXA6 crystal structure may be considered equivalent to human ANXA6 (*56*−*58*). Docking simulation indicated that the most accessible site for a nucleotide was located in the center of bovine ANXA6. Around this center, a box (delimited with yellow spheres and black lines) with an edge length of 2.2 nm surrounded the putative site, as indicated in Figure 6. The location of the putative nucleotide site within the box was also consistent with the experimental results, since both fragments contributed to the binding of the nucleotide. Therefore, the intersection of ANXA6a (green-colored backbone) and ANXA6b (blue-colored backbone) (Figure 6) should correspond to the nucleotide-binding site of the whole ANXA6.

The nucleotide was allowed to move at random within the box, and its conformation was allowed to be flexible; the structure of the ANXA6 protein remained rigid during the molecular modeling calculations by fixation on a grid. The best result of the simulation of the binding of GTP to bovine ANXA6 is presented in Figure 7, where K296, Y297, Q341, M342, S346, K598, L602, and K644 (numbering of amino acid residues was based on the full sequence containing an initial M according to ANXA6 coordinates; see ref *41*) were separated by less than 3 Å from the nucleotide. For the sake of the comparison, only lysine and tyrosine residues are shown in Figure 7. The purine and the ribose moieties of the GTP molecule were found to be relatively flexible. In contrast, the β- and γ-phosphate groups were found to be located within the same region, as inferred from several sets of simulations. This was also confirmed by simulation on binding of ATP to ANXA6 (Figure 8). Indeed, the two phosphate groups of ATP pointed toward the same binding site as the phosphate groups of GTP, while their respective purine and ribose groups were more flexible. The W343 residue was separated by ∼4 Å from the nucleotide, and it was possibly involved in guiding the purine moiety of the nucleotide to the binding site.

A tentative phosphate-binding motif was inferred on the basis of the simulation of bovine ANXA6: K296-Y297...Q341-M342-W343-XX-S346...K598-XXX-L602...K644-Y645 (numbering of amino acid residues was based on the full sequence containing the initial M). Searching the

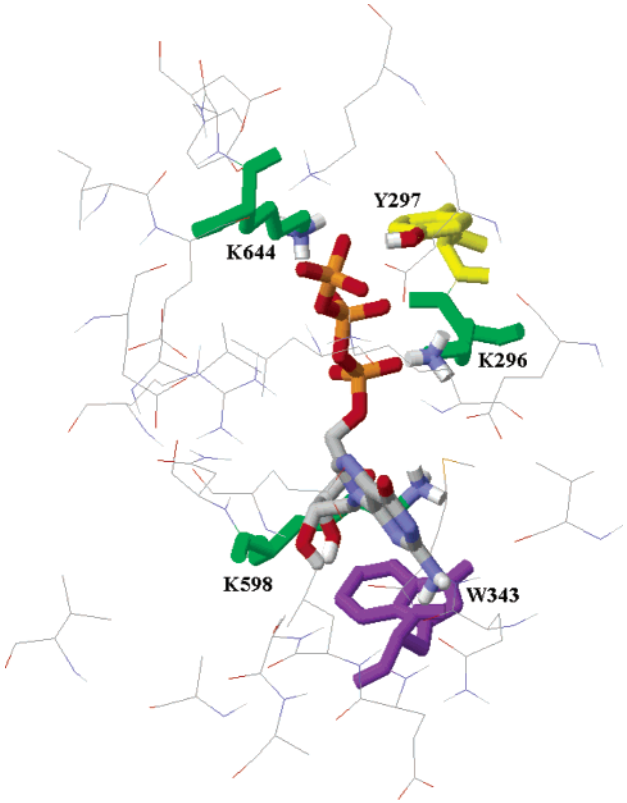

FIGURE 7: Close-up view of the GTP-binding site. Probable location of GTP in bovine ANXA6, based on the molecular simulation. The purine and ribose groups are relatively flexible, while phosphate groups are tightly bound to lysine (K644 and K296) and tyrosine (Y297) residues, which are less than 3 Å from the nucleotide. The tryptophan residue, W343, is in the vicinity of the purine moiety of GTP.

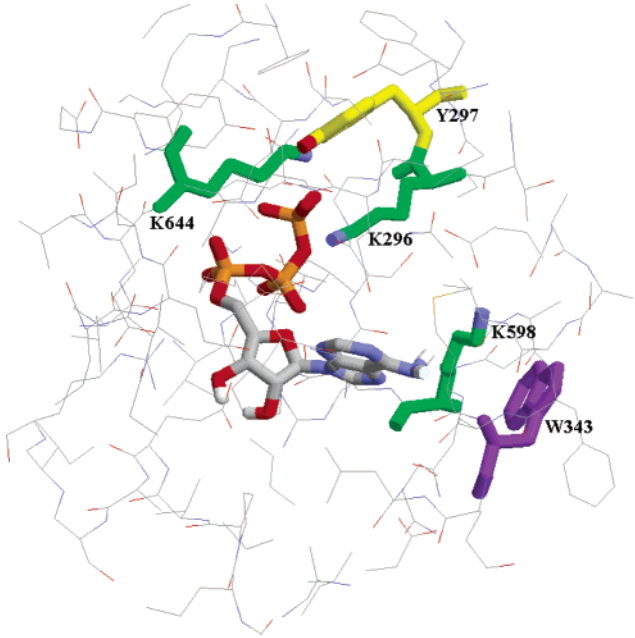

FIGURE 8: Close-up view of the ATP-binding site. Probable location of ATP in bovine ANXA6, based on the molecular simulation. The phosphate groups are tightly bound to lysine (K644 and K296) and tyrosine (Y297) residues, which are less than 3 Å from the nucleotide. However, the purine and the sugar moieties are more flexible.

sequence of the eight-repeat domains of human annexin and comparison with the sequences of mammalian ANXA6, we found two identical sequences in human and bovine ANXA6 with the F-X-X-K-Y-D/E-K-S-L motif. The sequences are residues 293−301 and 641−649 (numbering according to human and bovine sequences, including the initial M) (Figure 9).

DISCUSSION

Phosphate Binding Induced Small Structural Changes in Human ANXA6. The results of this work utilizing RIDS suggest that the interactions between phosphate and ANXA6 were small. As probed by RIDS, the structural alterations are observed in only six or seven amino acid residues of ANXA6. Similar RIDS spectra (similar band shapes with different magnitudes) are observed during the interactions of porcine liver ANXA6 with caged-ATP (*4*), as well as in the case of the binding of GTP-γ-S to human recombinant ANXA6 examined with caged-GTP-γ-S (*5*). One possible interpretation of these results is that the interactions between nucleotides and ANXA6 are mainly due to the phosphate groups of the nucleotide. These interactions with the protein induce only a slight distortion of the α-helical structures (as characterized by the change around 1652−1656 cm^{-1}) and/or the formation of stronger hydrogen bonds involving carbonyl groups of the peptide backbone (corresponding to a shift from 1652−1656 to 1621 cm^{-1}). The involvement of phosphate groups of the nucleotide moiety has been proposed for the binding of GTP to Ras protein (*59*, *60*), and binding of ATP to Ca^{2+}-ATPase (*61*), arginine kinase (*62*), and to creatine kinase (*63*).

Nucleotide-Binding Site of Human ANXA6. To locate a putative nucleotide-binding site(s) of ANXA6, the nucleotide binding properties of ANXA6a and ANXA6b were determined. The RIDS spectrum of ANXA6a with caged-GTP-γ-S in the presence of Ca^{2+} was similar to the RIDS spectrum of ANXA6, but its amplitude was equal to half the amplitude of ANXA6, measured under the same conditions and same molar concentrations (Figure 4). This suggested that half of the amino acid residues, e.g., four or five, were affected upon GTP-γ-S binding to ANXA6a, as compared with eight or nine amino acid residues for the whole annexin (Table 1). RIDS of the other fragment (ANXA6b) with caged-GTP-γ-S in the presence of Ca^{2+} also yields a RIDS spectrum similar to but smaller than that for ANXA6 (Figure 4), indicating that three or four amino acid residues are involved during binding of GTP-γ-S to the C-terminal fragment of ANXA6 (Table 1). The similarities in the RIDS spectra of both fragments of ANXA6 suggest that there are at least two nucleotide-binding sites located in a similar environment. The environment of a nucleotide-binding site of ANXA6 contained amino acid residues which are located in both N-terminal and C-terminal regions of ANXA6. This is corroborated by the fluorescence measurements using TNP-GTP as a probe of the nucleotide binding properties of ANXA6, ANXA6a, and ANXA6b. Our fluorescence results are consistent with previous findings (*4*) that the stoichiometry of nucleotide binding with ANXA6 is 1:1. TNP-GTP binds to both ANXA6 fragments with a nucleotide:ANXA6a or nucleotide:ANXA6b stoichiometry (moles per mole) of 0.5:1, although there is a striking difference in TNP-GTP binding parameters between both halves of ANXA6. The 0.5:1 stoichiometry (moles per mole) for the nucleotide−ANXA6a or −ANXA6b complexes may indicate a dimer

Human	A2	(303-319)	I	R	S	E	F	K	R	K	Y	G	K	S	L	Y	Y	Y	I
Human	A3	(128-144)	I	S	Q	A	Y	Y	T	V	Y	K	K	S	L	G	D	D	I
Human	A4	(283-299)	I	R	A	H	F	K	R	L	Y	G	K	S	L	Y	S	F	I
Human	A6	(130-146)	L	V	A	A	Y	K	D	A	Y	E	R	D	L	E	A	D	I
Human	A6	(289-305)	I	R	E	I	F	R	T	K	Y	E	K	S	L	Y	S	M	I
Human	A6	(473-489)	I	N	E	A	Y	K	E	D	Y	H	K	S	L	E	D	A	L
Human	A6	(637-653)	I	R	R	E	F	I	E	K	Y	D	K	S	L	H	Q	A	I
Human	A9	(301-317)	I	R	A	E	F	R	K	K	F	G	K	S	L	Y	S	S	L
Human	A10	(285-301)	I	R	K	R	Y	K	E	R	Y	G	K	S	L	F	H	D	I
Human	A11	(469-485)	I	R	S	E	Y	K	R	M	Y	G	K	S	L	Y	H	D	I
Human	A13	(283-299)	I	K	A	K	F	Q	E	K	Y	Q	K	S	L	S	D	M	V
Bovine	A6	(289-305)	I	R	E	I	F	R	T	K	Y	E	K	S	L	Y	S	M	I
Bovine	A6	(637-653)	I	R	R	E	F	I	E	K	Y	D	K	S	L	H	Q	A	I
consensus sequence			-	-	-	-	F/Y	X	X	X	Y/F	X	K	S	L	-	-	-	-

FIGURE 9: Multiple-sequence alignment of the mammalian annexin family in the putative phosphate binding region. In the case of ANXA6, four repeat sequences are shown.

binding one nucleotide molecule. Dimer formation has been reported for bovine kidney ANXA4, four-repeat domain annexin which can form dimers in solution cross-linked at C198 via a disulfide bond (*64*). To the best of our knowledge, such dimers have not been described so far for eight-repeat domain ANXA6.

Consensus Sequence for Phosphate Recognition by Human ANXA6. To perform molecular modeling simulations, the nucleotide was allowed to bind in the center of bovine ANXA6 in a box of limited dimensions with an edge length of 2.2 nm. The location and the dimension of the box are consistent with experimental results, as well as with the position of the most accessible cavities. The simulations, either with GTP or with ATP, indicate that the locations of β- and γ-phosphate-binding sites of ANXA6 are identical despite the fact that their purine and ribose moieties are relatively flexible and are randomly oriented. This would suggest that the β- and γ-phosphate chains are tightly bound to ANXA6, while the other parts of the nucleotide interact weakly with the protein. This is in agreement with the results of RIDS indicating that structural changes are caused mostly by the phosphate groups. By comparing the relative magnitudes of the RIDS spectra obtained for caged-ATP and caged-P_i and by using molecular modeling, we can extrapolate that approximately one or two phosphate groups can bind to ANXA6 after photorelease from caged-P_i. A close analysis of the surrounding residues (K296, Y297, and K644 are less than 3 Å from the nucleotide; see Figures 7 and 8) has allowed us to propose a tentative motif for the nucleotide-binding site of ANXA6. In the case of human and bovine ANXA6, two identical F-X-X-K-Y-D/E-K-S-L sequences, residues 293−301 (within annexin repeat domain IV) and residues 641−649 (within annexin repeat domain VIII), are present (Figure 9). This is consistent with the idea that both the N- and C-terminal parts of ANXA6 participate in the phosphate binding site. Fragments ANXA6a (with repeat domain IV) and ANXA6b (containing repeat domain VIII) bind GTP-γ-S, despite the fact that they represent only half of the binding site. Both these sequences contain carboxylate residues of either E298 or D646 in the vicinity of reactive K-Y residues. Consitent with this, RIDS of fragments ANXA6a and ANXA6b, as well as the whole ANXA6, suggests the involvement of the carboxylate group during nucleotide or phosphate binding, as evidenced by their spectral changes arround 1579 cm^{-1} (Figure 4).

A search for a consensus sequence, present in other annexins, shows that the F-X-X-K-Y-D/E-K-S-L motif is not completely conserved in all annexins. However, a more general sequence containing the less restricted motif F/Y-X-X-X-F/Y-X-K-S-L is present in other human annexins: ANXA2−ANXA4, ANXA9−ANXA11, and ANXA13. The F/Y-X-X-X-F/Y-X-K-S-L motif may originate from a common ancestor and may have some functional properties which could be modulated by the subtle amino acid substitutions. Q341, M342, W343, and S346 are located in the vicinity of the nucleotide-binding site of ANXA6, although there is no consensus sequence associated with these residues in other annexin families to support a characteristic binding site.

Comparison with the Membrane Recognition Domain of Annexins. Recently, a new consensus sequence RXXXK for phosphatidylserine recognition by ANXA5 (*65*) has been reported. The RXXXK motif is responsible for the interactions involving negatively charged serine and phosphate groups of phosphatidylserine (*65*). This motif is found in the middle of the consensus F/Y-X-X-X-F/Y-X-K-S-L sequence of ANXA2 (F-K-R-K-Y-G-K-S-L) and ANXA4 (F-K-R-L-Y-G-K-S-L) (Figure 9), consistent with the idea that this motif is important for phosphate binding. The differences in the F/Y-X-X-X-F/Y-X-K-S-L sequence among annexin subfamilies may affect the fine-tuning functional properties, altering the nucleotide−annexin and/or calcium-induced phosphatidylserine−annexin interactions.

ACKNOWLEDGMENT

We thank Professor R. Huber from the Max-Planck-Institut fur Biochemie (Martinsried, Germany) for providing cDNA for human annexin ANXA6 and Professor R. Donato from Universita di Perugia (Perugia, Italy) for sending *E. coli* transformed with ANXA6 cDNA. We acknowledge fruitful discussion with Professor Yogesh C. Awasthi (Department of Human Biological Chemistry and Genetics, University of Texas Medical Branch at Galveston, Galveston, TX).

REFERENCES

1. Morgan, R. O., Jenkins, N. A., Gilbert, D. J., Copeland, N. G., Balsara, B. R., Testa, J. R., and Fernandez, M. P. (1999) Novel human and mouse annexin A10 are linked to the genome duplications during early chordate evolution, *Genomics 60*, 40−49.
2. Bandorowicz-Pikula, J., and Awasthi, Y. C. (1997) Interaction of annexins IV and VI with ATP. An alternative mechanism by which

a cellular function of these calcium- and membrane-binding proteins is regulated, *FEBS Lett. 409*, 300−306.
3. Bandorowicz-Pikula, J., Wrzosek, A., Pikula, S., and Awasthi, Y. C. (1997) Fluorescence spectroscopic studies on interactions between liver annexin VI and nucleotides: a possible role for a tryptophan residue, *Eur. J. Biochem. 248*, 238−244.
4. Bandorowicz-Pikula, J., Wrzosek, A., Danieluk, M., Pikula, S., and Buchet, R. (1999) ATP-Binding site of annexin VI characterized by photochemical release of nucleotide and infrared difference spectroscopy, *Biochem. Biophys. Res. Commun. 263*, 775−779.
5. Kirilenko, A., Golczak, M., Pikula, S., Buchet, R., and Bandorowicz-Pikula, J. (2002) GTP-induced membrane binding and ion channel activity of annexin VI: is annexin VI a GTP biosensor? *Biophys. J. 82*, 2737−2745.
6. Bandorowicz-Pikula, J. (1998) A nucleotide-binding domain of porcine liver annexin VI. Proteolysis of annexin VI labelled with 8-azido-ATP, purification by affinity chromatography on ATP-agarose, and fluorescence studies, *Mol. Cell. Biochem. 181*, 11−20.
7. Bandorowicz-Pikula, J., Buchet, R., and Pikula, S. (2001) Annexins as nucleotide-binding proteins: facts and speculations, *BioEssays 23*, 170−178.
8. Gerke, V., and Moss, S. E. (2002) Annexins: from structure to function, *Physiol. Rev. 82*, 331−371.
9. Babiychuk, E. B., and Draeger, A. (2000) Annexins in cell membrane dynamics. Ca^{2+}-regulated association of lipid microdomains, *J. Cell Biol. 150*, 1113−1123.
10. Coleman, R., and Roma, M. G. (2000) Hepatocyte couplets, *Biochem. Sci. Trans. 28*, 136−140.
11. Turpin, E., Russo-Marie, F., Dubois, T., de Paillerets, C., Alfsen, A., and Bomsel, M. (1998) In adrenocortical tissue, annexins II and VI are attached to clathrin coated vesicles in a calcium-independent manner, *Biochim. Biophys. Acta 1402*, 115−130.
12. Schnitzer, J. E., Liu, J., and Oh, P. (1995) Endothelial caveolae have the molecular transport machinery for vesicle budding, docking, and fusion including VAMP, NSF, SNAP, annexins, and GTPases, *J. Biol. Chem. 270*, 14399−14404.
13. Davis, A. J., Butt, J. T., Walker, J. H., Moss, S. E., and Gawler, D. J. (1996) The Ca^{2+}-dependent lipid binding domain of $p120^{GAP}$ mediates protein−protein interactions with Ca^{2+}-dependent membrane-binding proteins. Evidence for a direct interaction between annexin VI and $p120^{GAP}$, *J. Biol. Chem. 271*, 24333−24336.
14. Chow, A., Davis, A. J., and Gawler, D. J. (2000) Identification of a novel protein complex containing annexin VI, Fyn, Pyk2, and the $p120^{GAP}$ C2 domain, *FEBS Lett. 469*, 88−92.
15. Calvert, C. M., Gant, S. J., and Bowles, D. J. (1996) Tomato annexins p34 and p35 bind to F-actin and display nucleotide phosphodiesterase activity inhibited by phospholipid binding, *Plant Cell 8*, 333−342.
16. McClung, A. D., Carroll, A. D., and Battey, N. H. (1996) Identification and characterization of ATPase activity associated with maize (*Zea mays*) annexins, *Biochem. J. 303*, 709−712.
17. Shin, H., and Brown, R. M., Jr. (1999) GTPase activity and biochemical characterization of a recombinant cotton fiber annexin, *Plant Physiol. 119*, 925−934.
18. Clark, G. B., Sessions, A., Eastburn, D. J., and Roux, S. J. (2001) Differential expression of members of the annexin multigene family in *Arabidopsis*, *Plant Physiol. 126*, 1072−1084.
19. Hofmann, A., Proust, J., Dorowski, A., Schantz, R., and Huber, R. (2000) Annexin 24 from *Capsicum annuum*. X-ray structure and biochemical characterization, *J. Biol. Chem. 275*, 8072−8082.
20. Caohuy, H., Srivastava, M., and Pollard, H. B. (1996) Membrane fusion protein synexin (annexin VII) as a Ca^{2+}/GTP sensor in exocytotic secretion, *Proc. Natl. Acad. Sci. U.S.A. 93*, 10797−10802.
21. Pollard, H. B., Caohuy, H., Minton, A. P., and Srivastava, M. (1998) Synexin (annexin VII) hypothesis for Ca^{2+}/GTP-regulated exocytosis, *Adv. Pharmacol. 42*, 81−87.
22. Caohuy, H., and Pollard, H. B. (2001) Activation of annexin 7 by protein kinase C *in vitro* and *in vivo*, *J. Biol. Chem. 276*, 12813−12821.
23. Caohuy, H., and Pollard, H. B. (2002) Protein kinase C and guanosine triphosphate combine to potentiate calcium-dependent membrane fusion driven by annexin 7, *J. Biol. Chem. 277*, 25217−25225.
24. Chander, A., Sen, N., and Spitzer, A. R. (2001) Synexin and GTP increase surfactant secretion in permeabilized alveolar type II cells, *Am. J. Physiol. 280*, L991−L998.
25. Danieluk, M., Golczak, M., Pikula, S., and Bandorowicz-Pikula, J. (2001) UDP hydrolase activity associated with the porcine liver annexin fraction, *Biochim. Biophys. Acta 1526*, 70−76.
26. Barth, A., and Zscherp, C. (2000) Substrate binding and enzyme function investigated by infrared spectroscopy, *FEBS Lett. 477*, 151−156.
27. Cepus, V., Ulbrich, C., Allin, C., Trouiller, A., and Gerwert, K. (1998) Fourier transform infrared photolysis studies of caged compounds, *Methods Enzymol. 291*, 223−245.
28. Mäntele, W. (1993) Reaction-induced infrared difference spectroscopy for the study of protein function and reaction mechanisms, *Trends Biochem. Sci. 18*, 197−202.
29. Siebert, F. (1995) Infrared spectroscopy applied to biochemical and biological problems, *Methods Enzymol. 246*, 501−526.
30. Zscherp, C., and Barth, A. (2001) Reaction-induced infrared difference spectroscopy for the study of protein reaction mechanisms, *Biochemistry 40*, 1875−1883.
31. Burger, A., Berendes, R., Voges, D., Huber, R., and Demange, P. (1993) A rapid and efficient purification method for recombinant annexin V for biophysical studies, *FEBS Lett. 329*, 25−28.
32. Golczak, M., Kirilenko, A., Bandorowicz-Pikula, J., and Pikula, S. (2001) Conformational states of annexin VI in solution induced by acidic pH, *FEBS Lett. 496*, 49−54.
33. Golczak, M., Kirilenko, A., Bandorowicz-Pikula, J., and Pikula, S. (2001) N- and C-terminal halves of human annexin VI differ in ability to form low pH-induced ion channels, *Biochem. Biophys. Res. Commun. 284*, 785−791.
34. Sanger, F., Nicklen, S., and Coulson, A. R. (1977) DNA sequencing with chain-terminating inhibitors, *Proc. Natl. Acad. Sci. U.S.A. 74*, 5463−5467.
35. Glasoe, P. K., and Long, F. A. (1960) Use of glass electrodes to measure acidities in deuterium oxide, *J. Phys. Chem. 64*, 188−190.
36. Barth, A., von Germar, F., Kreutz, W., and Mäntele, W. (1996) Time-resolved infrared spectroscopy of the Ca^{2+}-ATPase. The enzyme at work, *J. Biol. Chem. 271*, 30637−30646.
37. Scheirlinckx, F., Buchet, R., Ruysschaert, J. M., and Goormaghtigh, E. (2001) Monitoring of secondary and tertiary structure changes in the gastric H^+/K^+-ATPase by infrared spectroscopy, *Eur. J. Biochem. 268*, 3644−3653.
38. Lakovicz, J. R. (1983) *Principles of fluorescence spectroscopy*, Plenum, New York.
39. Huang, S. G., and Klingenberg, M. (1995) Fluorescent nucleotide derivatives as specific probes for the uncoupling protein: thermodynamics and kinetics of binding and the control by pH, *Biochemistry 34*, 349−360.
40. Huang, S. G., Weisshart, K., and Fanning, E. (1998) Characterization of the nucleotide binding properties of SV40 T antigen using fluorescent 3′(2′)-*O*-(2,4,6-trinitrophenyl)adenine nucleotide analogues, *Biochemistry 37*, 15336−15344.
41. Avila-Sakar, A. J., Creutz, C. E., and Kretsinger, R. H. (1998) Crystal structure of bovine annexin VI in a calcium-bound state, *Biochim. Biophys. Acta 1387*, 103−116.
42. Brady, G. P., Jr., and Stouten, P. F. W. (2000) Fast prediction and visualization of protein binding pockets with PASS, *J. Comput.-Aided Mol. Des. 14*, 383−401.
43. Morris, G. M., Goodsell, D. S., Halliday, R. S., Huey, R., Hart, W. E., Belew, R. K., and Olson, A. J. (1998) Automated docking using a Lamarckian genetic algorithm and an empirical binding free energy function, *J. Comput. Chem. 14*, 1639−1662.
44. Bradford, M. M. (1976) A rapid and sensitive method for the quantitation of microgram quantities of protein utilizing the principle of protein-dye binding, *Anal. Biochem. 72*, 248−254.
45. Schoenmakers, T. J. M., Visser, G. J., Flik, G., and Theuvenet, A. P. R. (1992) CHELATOR: an improved method for computing metal ion concentrations in physiological solutions, *BioTechniques 12*, 870−874.
46. Laemmli, U. K. (1970) Cleavage of structural proteins during the assembly of the head of bacteriophage T4, *Nature 227*, 680−685.
47. Byler, D. M., and Susi, H. (1986) Examination of the secondary structure of proteins by deconvolved FTIR spectra, *Biopolymers 25*, 469−487.
48. Surewicz, W. K., Mantsch, H. H., and Chapman, D. (1993) Determination of protein secondary structure by Fourier transform infrared spectroscopy: a critical assessment, *Biochemistry 32*, 389−394.

49. Yang, J.-T., Wu, C.-S. C., and Martinez, H. M. (1986) Calculation of protein conformation from circular dichroism, *Methods Enzymol. 130*, 208−269.
50. Wu, F., Gericke, A., Flach, C. R., Mealy, T. R., Seaton, B. A., and Mendelsohn, R. (1998) Domain structure and molecular conformation in annexin V/1,2-dimyristoyl-*sn*-glycero-3-phosphate/Ca^{2+} aqueous monolayers: a Brewster angle microscopy/infrared reflection−absorption spectroscopy study, *Biophys. J. 74*, 3273−3281.
51. Wu, F., Flach, C. R., Seaton, B. A., Mealy, T. R., and Mendelsohn, R. (1999) Stability of annexin V in ternary complexes with Ca^{2+} and anionic phospholipids: IR studies of monolayer and bulk phases, *Biochemistry 38*, 792−799.
52. Silvestro, L., and Axelsen, P. H. (1999) Fourier transform infrared linked analysis of conformational changes in annexin V upon membrane binding, *Biochemistry 38*, 113−121.
53. Barth, A. (2000) The infrared absorption of amino acid side chains, *Prog. Biophys. Mol. Biol. 74*, 141−173.
54. Chirgadze, Y. N., Fedorov, O. V., and Trushina, N. P. (1975) Estimation of amino acid residue side-chain absorption in the infrared spectra of protein solutions in heavy water, *Biopolymers 14*, 679−694.
55. Goormaghtigh, E., Cabiaux, V., and Ruysschaert, J. M. (1994) Determination of soluble and membrane protein structure by Fourier Transform Infrared Spectroscopy. I. Assignments and model compounds, in *Physical Methods in the Study of Biomembranes* (Hilderson, H. J., and Ralston, G. B., Eds.) Vol. 23, pp 329−362, Plenum Press, New York.
56. Freye-Minks, C., Kretsinger, R. H., and Creutz, C. E. (2003) Structural and dynamic changes in human annexin VI induced by a phosphorylation-mimicking mutation, T356D, *Biochemistry 42*, 620−630.
57. Benz, J., Bergner, A., Hofmann, A., Demange, P., Göttig, P., Liemann, S., Huber, R., and Voges, D. (1996) The structure of recombinant human annexin VI in crystals and membrane-bound, *J. Mol. Biol. 260*, 638−643.
58. Avila-Sakar, A. J., Kretsinger, R. H., and Creutz, C. E. (2000) Membrane-bound 3D structures reveal the intrinsic flexibility of annexin VI, *J. Struct. Biol. 30*, 54−62.
59. Cepus, V., Scheidig, A. J., Goody, R. S., and Gerwert, K. (1998) Time-resolved FTIR studies of the GTPase reaction of H-ras p21 reveal a key role for the β-phosphate, *Biochemistry 37*, 10263−10271.
60. Allin, C., and Gerwert, K. (2001) Ras catalyzes GTP hydrolysis by shifting negative charges from γ- to β-phosphate as revealed by time-resolved FTIR difference spectroscopy, *Biochemistry 40*, 3037−3046.
61. Von Germar, F., Barth, A., and Mäntele, W. (2000) Structural changes of the sarcoplasmic reticulum Ca^{2+}-ATPase upon nucleotide binding studied by Fourier transform infrared spectroscopy, *Biophys. J. 78*, 1531−1540.
62. Raimbault, C., Besson, F., and Buchet, R. (1997) Conformational changes of arginine kinase induced by photochemical release of nucleotides from caged nucleotides: an infrared difference-spectroscopy investigation, *Eur. J. Biochem. 244*, 343−351.
63. Raimbault, C., Buchet, R., and Vial, C. (1996) Changes of creatine kinase secondary structure induced by the release of nucleotides from caged compounds. An infrared difference-spectroscopy study, *Eur. J. Biochem. 240*, 134−142.
64. Kojima, K., Yamamoto, K., Irimura, T., Osawa, T., Ogawa, H., and Matsumoto, I. (1996) Characterization of carbohydrate-binding protein p33/41: relation with annexin IV, molecular basis of the doublet forms (p33 and p41), and modulation of the carbohydrate binding activity by phospholipids, *J. Biol. Chem. 271*, 7679−7685.
65. Montaville, P., Neumann, J.-M., Russo-Marie, F., Oschsenbein, F., and Sanson, A. (2002) A new consensus sequence for phosphatidylserine recognition by annexins, *J. Biol. Chem. 277*, 24684−24693.

BI034359M